

Simulations on High- z Long Gamma-Ray Burst Rate

Shu-Fu Qin¹, En-Wei Liang^{1*}, Rui-Jing Lu¹, Jian-Yan Wei², Shuang-Nan Zhang^{3,4}

¹*Department of Physics, Guangxi University, Nanning 530004, China*

²*National Astronomical Observatories, Chinese Academy of Sciences, 100012 Beijing, China*

³*Key Laboratory of Particle Astrophysics, Institute of High Energy Physics, Chinese Academy of Sciences, Beijing 100049, China*

⁴*Physics Department, University of Alabama in Huntsville, Huntsville, AL 35899, USA*

21 August 2018

ABSTRACT

Since the launch of *Swift* satellite, the detections of high- z ($z > 4$) long gamma-ray bursts (LGRBs) have been rapidly growing, even approaching the very early Universe (the record holder currently is $z=8.3$). The observed high- z LGRB rate shows significant excess over that estimated from the star formation history. We investigate what may be responsible for this high productivity of GRBs at high- z through Monte Carlo simulations, with effective *Swift*/BAT trigger and redshift detection probabilities based on current *Swift*/BAT sample and *CGRO*/BATSE LGRB sample. We compare our simulations to the *Swift* observations via $\log N - \log P$, peak luminosity (L) and redshift distributions. In the case that LGRB rate is purely proportional to the star formation rate (SFR), our simulations poorly reproduce the LGRB rate at $z > 4$, although the simulated $\log N - \log P$ distribution is in good agreement with the observed one. Assuming that the excess of high- z GRB rate is due to the cosmic metallicity evolution or unknown LGRB rate increase parameterized as $(1+z)^\delta$, we find that although the two scenarios alone can improve the consistency between our simulations and observations, incorporation of them gives much better consistency. We get $0.2 < \epsilon < 0.6$ and $\delta < 0.6$, where ϵ is the metallicity threshold for the production of LGRBs. The best consistency is obtained with a parameter set $(\epsilon, \delta) = (\sim 0.4, \sim 0.4)$, and BAT might trigger a few LGRBs at $z \simeq 14$. With increasing detections of GRBs at $z > 4$ ($\sim 15\%$ of GRBs in current *Swift* LGRB sample based on our simulations), a window for very early Universe is opening by *Swift* and up-coming SVOM missions.

Key words: gamma-rays: bursts methods: simulations gamma-rays: observations

1 INTRODUCTION

Gamma-ray bursts (GRBs) are the most luminous events in the Universe. They may be detected out to distance of $z > 10$ (Lamb & Reichart 2000; Bromm & Loeb 2002; Gou et al. 2004; Lin et al. 2004). It is believed that long GRBs (LGRBs) with $T_{90} > 2$ s (Kouveliotou et al. 1993) are from the death of massive stars (e.g., Woosley 1993; Paczynski 1998; Woosley & Bloom 2006), hence their rate may trace the star formation rate (SFR) (Totani 1997; Wijers et al. 1998; Lamb & Reichart 2000; Blain & Natarajan 2000; Porciani & Madau 2001; Zhang & Mészáros 2004; Piran 2004; Zhang 2007). Simulations for this scenario can roughly reproduce the observed luminosity (L), redshift, and $\log N - \log P$ distributions (e.g., Liang et al. 2007; Virgil et al. 2009a,b), however, evidence that LGRBs do not follow star formation unbiasedly has been growing with rapidly increasing number of high- z GRBs detected with *Swift*/BAT

(e.g., Daigne et al. 2006; Le & Dermer 2007; Yüksel & Kistler 2007; Salvaterra & Chincarini 2007; Guetta & Piran 2007; Salvaterra et al. 2008; Kistler et al. 2008, 2009; Wang & Dai 2009). After the detection of GRB 050904 at $z = 6.29$ (Kawai et al. 2006; Haislip et al. 2006) three year later, other two higher- z LGRBs were detected, GRB 080913 at $z \sim 6.7$ (Greiner et al. 2009) and GRB 090423 at $z \sim 8.3$ (Tanvir et al. 2009). This ever-increasing number of detectable high- z LGRBs shows that the LGRB rate at high redshift may be higher than that expected previously. Kistler et al. (2008) found significant excess of the LGRB rate over the SFR at $z \approx 4$ based on a sample of 36 luminous LGRBs. They suggested that some unknown mechanisms lead to this observed enhance in the GRB rate, such as the cosmic evolutions of the metallicity history and LGRB luminosity function.

Cosmic chemical evolution predicts that LGRBs should occur preferentially in metal poor environment. From a theoretical point of view, this is not surprising since lower metallicity leads to weaker stellar winds and hence less angular momentum loss, more probably resulting in rapidly

* E-mail: lew@gxu.edu.cn

rotating cores in the stars, as required in the collapsar model for GRBs (e.g., Woosley 1993; MacFayden & Woosley 1999; Yoon & Langer 2005). With host galaxy observations (Fynbo et al. 2003; Conselice et al. 2005; Gorosabel et al. 2005; Chen et al. 2005; Starling et al. 2005; Fruchter et al. 2006; Fynbo et al. 2006; Mirabal et al. 2006), it is found that the metallicity of LGRB hosts are on average lower than that of core-collapse supernovae (Wolf & Podsiadlowski 2007). The *Swift* sample also suggests a modest propensity for low-metallicity, evidenced by an increase in the rate density with redshift (Butler et al. 2009). One major restriction of LGRBs to low metallicity is that LGRBs do not follow star formation in an unbiased manner and LGRB rate may peak at a significantly higher redshift than supernovae (Lin et al. 2004; Langer & Norman 2006; Firmani et al. 2006). Assuming that LGRB rate traces both the SFR and the metallicity evolution history, Li (2008) found that the observed redshift distribution of the *Swift* LGRBs can be reproduced with a fairly good accuracy.

It was also suggested that LGRBs may have experienced some sort of luminosity evolution with redshift, being more luminous in the past (Lloyd-Ronning et al. 2002; Firmani et al. 2004; Kocevski & Liang 2006; Salvaterra et al. 2008; Salvaterra et al. 2009) or having a higher efficiency of LGRB production rate by massive stars at high- z (Daigne, et al. 2006). This effect may also modify the observed LGRB rate.

This paper is dedicated to exploring what may be responsible for the high productivity of LGRBs at high- z through simulations. Four scenarios are tested: (A) A LGRB rate that purely follows SFR; (B) a LGRB rate that follows SFR in cooperation with some sort of LGRB rate evolving with redshift characterized as $(1+z)^\delta$ (Kistler et al. 2009); (C) a LGRB rate that follows SFR in cooperation with cosmic metallicity evolution (taking the form as Langer and Norman 2006); (D) a LGRB rate that follows the SFR in conjunction with both LGRB rate evolution and cosmic metallicity evolution. Throughout this paper a flat Universe with $H_0 = 71 \text{ km s}^{-1} \text{ Mpc}^{-1}$, $\Omega_M = 0.3$ and $\Omega_\Lambda = 0.7$ is assumed.

2 MODEL

The number of LGRBs per unit time at redshift $z \sim z + dz$ with luminosity $L \sim L + dL$ is given by

$$\frac{dN}{dt dz dL} = \frac{R_{\text{LGRB}}(z)}{1+z} \frac{dV(z)}{dz} \Phi(L), \quad (1)$$

where $R_{\text{LGRB}}(z)$ is the event rate of LGRB (in units of $\text{Gpc}^{-3} \text{ yr}^{-1}$) as a function of z , $(1+z)^{-1}$ accounts for the cosmological time dilation, $\Phi(L)$ is the LGRB luminosity function, and

$$\frac{dV}{dz} = \frac{c}{H_0} \frac{4\pi D_L^2}{(1+z)^2 [\Omega_M (1+z)^3 + \Omega_\Lambda]^{1/2}} \quad (2)$$

is the co-moving volume element at redshift z in a flat Λ CDM universe. The $D_L(z)$ is the luminosity distance at z . Considering an instrument with flux threshold P_{th} and an average solid angle Ω for the aperture flux, the number of LGRB triggers with peak luminosity in a range $[L_{\text{min}}, L_{\text{max}}]$

during an observational period T should be

$$N = \frac{\Omega T}{4\pi} \int_{L_{\text{min}}}^{L_{\text{max}}} \eta_t(P) \Phi(L) dL \int_0^{z_{\text{max}}} \frac{R_{\text{LGRB}}(z)}{1+z} \frac{dV(z)}{dz} dz, \quad (3)$$

where $\eta_t(P)$ is the trigger probability of a burst with observed peak flux P , given by $P = L/4\pi D_L^2(z)k$, where the k factor corrects the bolometric flux in the burst rest frame ($1-10^4$ keV in this analysis) into the observed flux in an instrument energy band with the spectral information. The z_{max} of a given burst with luminosity L is determined by the instrumental flux threshold P_{th} through $P_{\text{th}} = L/4\pi D_L^2(z_{\text{max}})k$.

As discussed in §1, we express the LGRB rate as a function of redshift with

$$R_{\text{LGRB}}(z) \propto R_{\text{SFR}}(z) f(z) \Theta(\epsilon, z), \quad (4)$$

where $R_{\text{SFR}}(z)$ is the star formation rate, $f(z)$ accounts for potential cosmological evolution effects, $\Theta(\epsilon, z)$ is the fractional mass density belonging to metallicity below ϵZ_\odot at a given z (Z_\odot is the solar metal abundance), and ϵ is determined by the metallicity threshold for the production of LGRBs. In our simulations, $f(z)$ is simplified to $f(z) = (1+z)^\delta$ as adopted by Kistler et al. (2009), and the $\Theta(\epsilon, z)$ follows the law (Langer & Norman 2006),

$$\Theta(\epsilon, z) = \frac{\hat{\Gamma}(\kappa + 2, \epsilon^\beta 10^{0.15\beta z})}{\Gamma(\kappa + 2)}, \quad (5)$$

where $\kappa = -1.16$ is the power-law index in the Schechter distribution function of galaxy stellar masses (Panter et al. 2004), $\beta = 2$ is the slope in the linear bisector fit to the galaxy stellar mass-metallicity relation (Savaglio 2006), and $\hat{\Gamma}(a, x)$ and $\Gamma(x)$ are the incomplete and complete gamma function, respectively. The value of ϵ varies from 0.2 to 0.6 (Modjaz et al. 2008, Li 2008).

The star formation history is not well constrained by data at high redshifts ($z > 4$). The current observed SFR rapidly increases at $z < 1$, keeps almost a constant up to $z = 4.0$, then drops at $z > 4$. The sharp drop at $z > 4$ may be due to large dust extinction at such high redshifts. We adopt a SFR parameterized as (Rowan-Robinson 1999; Hopkins & Beacom 2006),

$$R_{\text{SFR}}(z) = R_0 \begin{cases} (1+z)^{3.44} & z \leq z_{\text{peak}}, \\ (1+z_{\text{peak}})^{3.44} & z > z_{\text{peak}}, \end{cases} \quad (6)$$

where $z_{\text{peak}} = 1$ and R_0 is a normalization parameter. The slope of the segment $z \leq z_{\text{peak}}$ is the well-fitted parameter in Hopkins & Beacom (2006).

It was suggested that low luminosity GRBs (LL-GRBs) may be a distinct GRB population from high-luminosity GRBs (HL-GRBs) with much higher local event rate (Soderberg et al. 2004; Cobb et al. 2006; Liang et al. 2007; Chapman et al. 2007). Liang et al. (2007) proposed a two-component broken power-law to model the GRB luminosity function. They characterize the luminosity function for each GRB population as

$$\phi(L) = \phi_0 \left[\left(\frac{L}{L_b} \right)^{\alpha_1} + \left(\frac{L}{L_b} \right)^{\alpha_2} \right]^{-1}, \quad (7)$$

where ϕ_0 is a normalization constant to assure the integral over the luminosity function being equal to unity, and L_b is the break luminosity. We do not consider the cosmological

evolution of the luminosity function¹. The global luminosity function thus is given by

$$\Phi(L) = \Phi_0[\rho_0^{LL}\phi^{LL}(L) + \rho_0^{HL}\phi^{HL}(L)] \quad (8)$$

where Φ_0 is a normalization constant, ρ_0^{LL} and ρ_0^{HL} are the local rates of low and high luminosity LGRBs, respectively.

3 SWIFT GRB SAMPLE AND SWIFT/BAT TRIGGER PROBABILITY

In order to eliminate the selection effect of different instruments, we use only the LGRBs detected by *Swift*/BAT to form a homogeneous sample. As of 31 May 2009, *Swift* had detected 385 LGRBs, with redshift measurement for 124 GRBs. The peak fluxes, measurement redshift and the spectral information for the GRB in our sample are taken from the NASA website². The peak fluxes are measured on 1-s timescale. It is known that the GRB spectrum is adequately fit with a smooth broken power-law, the so-called Band function (Band et al. 1993). Because of the narrowness of the BAT energy band, the BAT data cannot adequately constrain the spectral parameters of GRBs, and the GRB spectra observed with BAT are well fitted with a simple power law, $N \propto \nu^{-\Gamma}$ (Zhang et al. 2007). Empirically, Γ is roughly correlated to the observed peak spectral energy E_p by $\log E_p = (2.76 \pm 0.07) - (3.61 \pm 0.26) \log \Gamma$ (Zhang et al. 2007; Sakamoto et al. 2009). We employ this empirical relation to estimate the E_p of *Swift* GRBs and correct the observed peak luminosity to a bolometric band ($1 - 10^4$ keV) assuming the low and high energy spectral indexes as $\Gamma_1 = 0.83$ and $\Gamma_2 = 2.35$ (Preece et al. 2000; Kaneko et al. 2006) for all *Swift* GRBs and simulated bursts.

Selection effects involved in a GRB sample may disguise its truly intrinsic distribution (Bloom 2003; Fiore et al. 2007; Kistler et al. 2008; Le & Dermer 2007; Coward 2007; Coward et al. 2008). Two kinds of selection effects are concerned in our simulations. One is the *Swift*/BAT GRB trigger and the other is the redshift determination through spectroscopy of the optical/NIR afterglow or of the GRB host galaxy. The first one affects the peak flux distribution of a GRB sample and the other one affects the $L - z$ distribution.

The *Swift*/BAT trigger is quite complex and its sensitivity for GRBs is very difficult to parameterize (Band 2006). Practically, a GRB with peak flux slightly over the instrument threshold would not always make a trigger. The BAT trigger rate is about 64 LGRBs per year per solid angle, roughly equal to that of BATSE (~ 67 LGRBs per year per solid angle, see Stern et al. 2001). Comparison of the peak flux distributions of the LGRBs detected with BAT and BATSE is shown in Fig. 1. The Kolmogorov-Smirnov Test (K-S test) yields a probability $p_{K-S} = 0.79$, indicating that the two distributions are statistically indistinguishable.

¹ The luminosity evolution with being luminous in the past (Lloyd-Ronning et al. 2002; Firmani et al. 2004; Kocevski & Liang 2006; Salvaterra et al. 2008; Salvaterra et al. 2009) may also result in an increase of GRB rate with redshift as $(1+z)^\delta$ (Kistler et al. 2008).

² <http://swift.gsfc.nasa.gov/docs/swift/archive/grb-table/>

Therefore the two detectors should have comparable sensitivity for LGRBs. We consequently use the same trigger probability of *Swift*/BAT as that of *CGRO*/BATSE.

Stern et al. (2001) scanned the off-line daily archival data from BATSE and identified 3713 LGRBs, of which 1916 LGRBs are triggered events. Assuming that the peak fluxes of both triggered and non-triggered GRBs are over the BATSE threshold, we define the trigger efficiency η_t of a GRB as a function of P with the ratio of trigger event number to the total detected event number (including both triggered and non-triggered events) in a peak flux bin $P + dP$. The result is shown in Fig. 2, where P is converted to *Swift* energy band [15, 150] keV with the observed spectral parameters. It is found that the instrument trigger threshold is roughly 0.2 photon $\text{s}^{-1} \text{cm}^{-2}$. η_t as a function of P can be parameterized as

$$\eta_t = \begin{cases} 5.0P^{3.85}, & P < 0.45 \\ 0.67(1.0 - 0.40/P)^{0.52}, & P \geq 0.45 \end{cases} \quad (9)$$

Note that η_t remains almost a constant at 67% for $P > 1$ counts $\text{cm}^{-2} \text{s}^{-1}$. Some non-triggered events are very bright (the strongest one is 24 ph $\text{cm}^{-2} \text{s}^{-1}$). This is due to the dead time when the trigger was disabled during data readouts or when *CGRO* passed through regions of very high ionospheric activity (Stern et al. 2001). This effect does not affect our our simulations. We use this trigger probability curve for *Swift*/BAT in our simulations.

Fiore et al. (2007) pointed out that about 30% of *Swift* GRBs have measured redshifts (124/385 in the current *Swift* GRB sample). In order to simulate a GRB sample with redshift measurement, we empirically model probability of redshift measurement for a BAT triggered burst. From the current GRB sample, redshifts are preferentially measured for brighter GRBs at lower redshifts. We show the redshift measurement probability η_z as a function of $\log(P)$ in Fig. 3, where the probabilities are calculated by the ratio of the number of GRBs with redshift measurement in each bin to the number of triggered GRBs in the corresponding bin. It is found that the probability of redshift measurement for the burst in our sample does not strongly depend on P . In fact, the redshift measurement is complicated, depending on many artificial effects, such as the optical follow-up, spectral line detection, etc (Bloom 2003). Even though, we still use an empirical function parameterized as

$$\eta_z = 0.26 + 0.032e^{1.61 \log P} \quad (10)$$

to simulate GRB samples with redshift measurement.

4 MONTE CARLO SIMULATIONS

Based on the model discussed above, we make simulations to re-produce the *Swift* observations. In our simulations, the model parameters are constrained with comparison of our simulations to observations. Note that the parameters of the LL-GRB luminosity function are similar to that reported by Liang et al. (2007), i.e., $\alpha_1^{LL} = 0$, $\alpha_2^{LL} = 3.0$, and $L_b^{LL} = 7.5 \times 10^{46}$ erg s^{-1} . For HL-GRBs, we find that $L_b^{HL} = 2.75 \times 10^{52}$ erg s^{-1} and $\alpha_1^{HL} = 1.36$ can well reproduce the observations at $L < L_b^{HL}$. This is roughly consistent with that reported by Stern et al. (2002), Schmidt (2001), and Lloyd-Ronning et al. (2004). We fix these parameters

in all cases we study below. The parameter α_2^{HL} are slightly adjustable, varying from 2.0 to 2.5, in order to get the best consistency between our simulations and observations for different cases. The ρ_0^{HL} is $\sim 1 \text{ Gpc}^{-3} \text{ year}^{-1}$ (e.g., Schmidt 2001; Stern et al. 2002; Lloyd-Ronning et al. 2004; Liang et al. 2007), but it was suggested that $\rho_0^{\text{LL}} = 100 \sim 1000 \text{ Gpc}^{-3} \text{ year}^{-1}$, much higher than ρ_0^{HL} (e.g., Cobb et al. 2006; Liang et al. 2007; Chapman et al. 2007). The ρ_0^{LL} is very uncertain, but it does not significantly affect the K-S test results since only a few low-luminosity GRBs in the simulated GRB sample. The ϵ and δ that describe the metallicity history and the GRB rate evolution, respectively, are free parameters. We search for the best model parameter sets by evaluating the consistency between the simulated P , L , and z distributions and the observed ones with the K-S test. A larger value of p_{K-S} indicates a better consistency. A value of $p_{K-S} > 0.1$ is generally acceptable to claim the statistical consistency, and a value of $p_{K-S} < 10^{-4}$ convincingly rejects the hypothesis of the consistency (e.g. Bloom 2003). For simulations for a given set of parameters, we first evaluate the consistency of the $\log N - \log P$ distribution for the simulated triggered sample since the L and z distributions suffer from the biases of redshift detection. By screening the simulated triggered sample with the redshift measurement probability curve the consistencies of the P , L and z distributions should be significantly improved (with $p_{K-S} > 0.1$) for a reasonable parameter set. The details of our procedure are described as follows.

(i) Simulate a GRB with luminosity L at redshift z , $\text{GRB}(L, z)$. The redshift is generated from the co-moving number density of GRBs at redshift $z + dz$, i.e.,

$$\mathfrak{R}(z) = \frac{R_{\text{LGRB}}(z) dV}{1+z} \frac{dV}{dz}, \quad (11)$$

and L is simulated with the probability distributions derived from Eq. 8. We take $[L_{\text{min}}, L_{\text{max}}] = [10^{45}, 10^{55}] \text{ erg s}^{-1}$ and a redshift range of $z = 0 - 20$.

(ii) Derive E'_p in the burst frame with the $L - E'_p$ relation,

$$E'_p \approx 200 \text{ keV} L_{52}^{1/2} / C, \quad (12)$$

where C is taken from a random distribution in the range of $[0.1, 1]$ (Liang et al. 2004). The photon indices prior and post the break energy are assumed to be 0.83 and 2.35, respectively. With the spectral information, we calculate the peak photon flux P in the BAT band that corresponds to an energy band $[15 \times (1+z), 150 \times (1+z)]$ in the burst frame. The simulated GRB then is characterized as $\text{GRB}(L, z, P)$.

(iii) Screen a mock GRB with the BAT trigger probability (Eq. 9). We get the trigger probability η_t of burst with peak flux P from Eq. 9 and generate a random number Q_t in the range $(0, 1)$. If $0 < Q_t < \eta_t$, we pick up this event as a triggered GRB.

(iv) Repeat the above steps to simulate a BAT-triggered GRB sample of 385 GRBs and evaluate the consistencies of its $\log N - \log P$ distribution with the BAT observations by the K-S test.

(v) Screen the simulated triggered sample (385 GRBs) with the redshift measurement probability curve (Eq. 10). To do so, we calculate the η_z value for a given burst, and generate a random number Q_z in the range $(0, 1)$. If $0 < Q_z < \eta_z$, we pick up this event as a triggered GRB with redshift detection.

(vi) Evaluate the consistencies of $\log N - \log P$, L and z distributions of the simulated known-redshift by the K-S test. In a reasonable parameter set these distributions should be greater agreement with the observations than that of the simulated triggered sample, i.e., with larger p_{K-S} values.

We create simulations for four cases as below. We present our selected simulation results in the following section. The selected model parameters and K-S test results are summarized in Table 1, and distributions are shown in Figs. 4-6 and 8. Our simulations show that the highest redshift of LGRBs that may be triggered with *Swift*/BAT is ~ 14 .

4.1 Case A: $R_{\text{LGRB}}(z) \propto R_{\text{SFR}}(z)$

This case is for the GRB rate that purely follows the SFR. This was performed by Virgili et al. (2009a). We make improvements in this case by considering the trigger probability and redshift detection probability in our simulations. Comparisons between simulations and *Swift* observations are shown in Fig. 4. It is found that our simulations well reproduce the observed $\log N - \log P$ distribution, yielding $p_{K-S} = 0.423$ and $p_{K-S} = 0.585$ for the triggered and known-redshift samples, respectively. However, the observed luminosity and redshift distributions are poorly reproduced. The simulated GRBs at $z \approx 1$ is significantly over-produced, but the GRBs at $z > 2$ have significant deficit. This case also over-produces the GRBs around $L = 10^{51} \text{ erg s}^{-1}$, and under-generates GRBs with $L > 10^{53} \text{ erg s}^{-1}$. The p_{K-S} for the $\log L$ and $\log z$ distributions are smaller than 0.01.

4.2 Case B: $R_{\text{LGRB}}(z) \propto R_{\text{SFR}}(z)\Theta(\epsilon, z)$

This case assumes that the GRB rate is proportional to the star formation history incorporating with the cosmic metallicity history. We find that $\epsilon \sim 0.5$ gives the best consistency. Our results are shown in Fig. 5. In general, the simulations for this case are more consistent with the observations than Case A. The $\log N - \log P$ distribution is well reproduced, with $p_{K-S} = 0.372$ and $p_{K-S} = 0.449$ for the simulations on the triggered and known-redshift samples, respectively. The consistency of the simulated luminosity distribution is also accepted, with $p_{K-S} = 0.052$ and $p_{K-S} = 0.292$ for the triggered and the known-redshift samples, respectively. However, the simulated z distributions are only marginally acceptable, with $p_{K-S} = 0.033$ and $p_{K-S} = 0.009$ for the simulations on the triggered and known-redshift samples, respectively. Note that the consistency of z distribution becomes much worse for the simulated known-redshift sample.

4.3 Case C: $R_{\text{LGRB}}(z) \propto R_{\text{SFR}}(z)f(z)$

This case assumes that the GRB rate follows the SFR in conjunction with some sort of GRB rate evolving with redshift characterized by $(1+z)^\delta$ (Kistler et al. 2009). We find that $\delta = 0.85$ can yield the best consistency. The results are shown in Fig. 6. This case well reproduces the observed $\log N - \log P$, z , and L distributions, with $p_{K-S} = 0.889, 0.242, 0.369$, respectively, for the simulations on the known-redshift samples, respectively. However, the consistency of the z and L distributions of the simulations for

the triggered sample are only marginally acceptable (with $p_{K-S} < 0.1$).

4.4 Case D: $R_{LGRB}(z) \propto R_{SFR}(z)f(z)\Theta(\epsilon, z)$

In this case we assume that the GRB rate follows the SFR incorporating with both GRB rate evolution and cosmic metallicity evolution. We search for the best δ and ϵ by means of a global K-S test probability defined as $p_{K-S} = p_{K-S}^P \times p_{K-S}^z \times p_{K-S}^L$, where p_{K-S}^P , p_{K-S}^z , and p_{K-S}^L are the probabilities of the K-S tests for the $\log N - \log P$, z , and L distributions of the simulated GRB sample with redshift measurement. The contours of $p_{K-S} \geq 0.1$ are shown in Fig. 7. We find that $0.2 < \epsilon < 0.6$ and $\delta < 0.6$ in case of $p_{K-S} \geq 0.1$. The parameter set $(\epsilon, \delta) = (\sim 0.4, \sim 0.4)$ produces the best consistency between our simulations and observations, as show in Fig. 8, yielding $p_{K-S}^P = 0.698$, $p_{K-S}^z = 0.294$ and $p_{K-S}^L = 0.209$ for the triggered sample and $p_{K-S}^P = 0.993$, $p_{K-S}^z = 0.843$ and $p_{K-S}^L = 0.966$ for the known-redshift sample.

5 DISCUSSION

As shown above, the observed excesses of both high- z GRB rate at $z > 4$ and luminous GRBs with $L > 10^{53}$ erg s $^{-1}$ over that predicted by assuming that the GRB rate simply traces the star formation rate (Case A), can be explained with the cosmic metallicity evolution (Case B) and an unknown GRB rate increase as $(1+z)^\delta$ (Case C).

Our simulations of Case D that incorporates Cases B and C well reproduce the observations. Taking this case as a preferred one, we find that the percentage of GRBs with $z > 4$ in the current BAT GRB sample is $\sim 15\%$ (~ 58 bursts) and $\sim 4\%$ of the GRBs (~ 15 bursts) have $z > 6$, consistent with that reported by Butler et al. (2009), but slightly larger than that predicted by (Daigne, et al. 2006). *Swift* has operated for five years. We thus simulate the observations for a 10 year operation. A uniform sample of ~ 1000 GRBs with ~ 300 redshift detections (in the current follow-up status) would be established in this mission period. Our simulations show that *Swift*/BAT-like instruments can trigger GRBs at redshift up to 14, and $\sim 0.5\%$ triggered *Swift* GRB may be at redshift $z > 10$. Exciting evidence is from *Swift* GRB 100205. The detected high red color of this GRB in its afterglows, $K-H=1.6 \pm 0.5$ mag, likely suggests that its redshift is $11 \leq z \leq 13.5$, if this red color is due to Lyman- α absorption within the H filter bandpass (Cucchiara et al. 2010). The era of exploring the deepest Universe with GRBs is coming, e.g., with rapid follow-up and localization capabilities on the ground and the space-based multi-band astronomical variable object monitor (SVOM) mission that is being developed in cooperation between the China and French (Götz et al. 2009; Basa, et al. 2008). Thanks to the low energy trigger threshold (~ 4 keV) of the ECLAIRS on-board, SVOM is more sensitive than previous missions for the detection of soft, hence potentially most distant, GRBs. The on-board visible telescope (VT) would quickly refine the GRB position for three ground based dedicated instruments, two robotic telescopes (GFTs) and a wide angle optical monitor (GWAC). Such optimized observing strategy would increase the redshift detection rate for high- z GRBs.

6 CONCLUSIONS

Motivated by the increasing detections of high- z GRBs, we have investigated what may be responsible for the high productivity of GRBs at high- z through Monte Carlo simulations. We parameterize the trigger probability of *Swift*/BAT using a large GRB sample observed with *CRGO*/BATSE. The redshift measurement probability is also derived from current *Swift* GRB sample. We compare our simulation results to the Swift observations with $\log N - \log P$ and $L - z$ distributions. We show in the case that the GRB rate is purely proportional to the SFR, our simulations poorly reproduce the GRBs rate at $z > 4$. We explain this GRB rate excess over that predicted by the SFR with the cosmic metallicity evolution effect and unknown GRB rate increase as $(1+z)^\delta$. Although the two scenarios can make better consistency between our simulations and observations, either one cannot simultaneously reproduce the observations alone. Incorporation of the two scenarios gives greater agreement between our simulations and observations, indicating that the combination of both GRB rate evolution and cosmic metallicity evolution would result in the observed high- z GRB rate excess over that predicted from the star formation history. We get $0.2 < \epsilon < 0.6$ and $\delta < 0.6$ in case of $p_{K-S} \geq 0.1$. The parameter set $(\epsilon, \delta) = (\sim 0.4, \sim 0.4)$ produces the best consistency between our simulations and observations. Our simulations show that the percentage of GRBs with $z > 4$ in the current BAT GRB sample is $\sim 15\%$, i.e., ~ 58 bursts, and a few triggered LGRBs may be at $z \simeq 14$. This is sufficient to make GRBs as promising probe for the high- z Universe.

ACKNOWLEDGMENTS

We appreciate valuable comments from the anonymous referee. We also thank Bing Zhang and Fransisco Virgili for helpful discussion. This work was supported by the National Natural Science Foundation of China under grants (No. 10873002, 10747001, 10821061, 10725313, and 10847003), and the National Basic Research Program (“973” Program) of China (Grant 2009CB824800), Guangxi SHI-BAI-QIAN project (Grant 2007201), the program for 100 Young and Middle-aged Disciplinary Leaders in Guangxi Higher Education Institution, and the research foundation of Guangxi University.

REFERENCES

- Band D., et al., 1993, ApJ, 413, 281
- Band D. L., 2006, ApJ, 644, 378
- Basa S., Wei J., Paul J., Zhang S. N., The Svom Collaboration, 2008, sf2a.conf, 161
- Blain A. W., Natarajan P., 2000, MNRAS, 312, L35
- Bloom J. S., 2003, AJ, 125, 2865
- Bromm V., Loeb A., 2002, ApJ, 575, 111
- Butler N. R., Bloom J. S., Poznanski D., 2009, arXiv, arXiv:0910.3341
- ucchiara, A., et al., 2010, GCN 10374
- Chapman R., Tanvir N. R., Priddey R. S., Levan A. J., 2007, MNRAS, 382, L21

- Chen H.-W., Prochaska J. X., Bloom J. S., Thompson I. B., 2005, *ApJ*, 634, L25
- Cobb B. E., Bailyn C. D., van Dokkum P. G., Natarajan P., 2006, *ApJ*, 645, L113
- Conselice C. J., et al., 2005, *ApJ*, 633, 29
- Coward D. M., Guetta D., Burman R. R., Imerito A., 2008, *MNRAS*, 386, 111
- Coward D., 2007, *NewAR*, 51, 539
- Daigne F., Rossi E. M., Mochkovitch R., 2006, *MNRAS*, 372, 1034
- Fiore F., Guetta D., Piranomonte S., D'Elia V., Antonelli L. A., 2007, *A&A*, 470, 515
- Firmani C., Avila-Reese V., Ghisellini G., Ghirlanda G., 2006, *MNRAS*, 372, L28
- Firmani C., Avila-Reese V., Ghisellini G., Tutukov A. V., 2004, *ApJ*, 611, 1033
- Fruchter A. S., et al., 2006, *Natur*, 441, 463
- Fynbo J. P. U., et al., 2003, *A&A*, 406, L63
- Fynbo J. P. U., et al., 2006, *A&A*, 451, L47
- Gorosabel J., et al., 2005, *A&A*, 444, 711
- Gou L. J., Mészáros P., Abel T., Zhang B., 2004, *ApJ*, 604, 508
- Götz D., et al., 2009, *AIPC*, 1133, 25
- Greiner J., et al., 2009, *ApJ*, 693, 1610
- Guetta D., Piran T., 2007, *JCAP*, 7, 3
- Haislip J. B., et al., 2006, *Natur*, 440, 181
- Hopkins A. M., Beacom J. F., 2006, *ApJ*, 651, 142
- Kaneko Y., Preece R. D., Briggs M. S., Paciasas W. S., Meegan C. A., Band D. L., 2006, *ApJS*, 166, 298
- Kawai N., et al., 2006, *Natur*, 440, 184
- Kistler M. D., Yüksel H., Beacom J. F., Hopkins A. M., Wyithe J. S. B., 2009, *ApJ*, 705, L104
- Kistler M. D., Yüksel H., Beacom J. F., Stanek K. Z., 2008, *ApJ*, 673, L119
- Kocevski D., Liang E., 2006, *ApJ*, 642, 371
- Kouveliotou C., Meegan C. A., Fishman G. J., Bhat N. P., Briggs M. S., Koshut T. M., Paciasas W. S., Pendleton G. N., 1993, *ApJ*, 413, L101
- Lamb D. Q., Reichart D. E., 2000, *ApJ*, 536, 1
- Langer N., Norman C. A., 2006, *ApJ*, 638, L63
- Le T., Dermer C. D., 2007, *ApJ*, 661, 394
- Li L.-X., 2008, *MNRAS*, 388, 1487
- Liang E. W., Dai Z. G., Wu X. F., 2004, *ApJ*, 606, L29
- Liang E. W., Zhang B., Virgili F., Dai Z. G., 2007, *ApJ*, 662, 1111
- Lin J. R., Zhang S. N., Li T. P., 2004, *ApJ*, 605, 819
- Lloyd-Ronning N. M., Fryer C. L., Ramirez-Ruiz E., 2002, *ApJ*, 574, 554
- Lloyd-Ronning N. M., Dai X., Zhang B., 2004, *ApJ*, 601, 371
- MacFadyen A. I., Woosley S. E., 1999, *ApJ*, 524, 262
- Mirabal N., Halpern J. P., An D., Thorstensen J. R., Terndrup D. M., 2006, *ApJ*, 643, L99
- Modjaz M., et al., 2008, *AJ*, 135, 1136
- Paczynski B., 1998, *ApJ*, 494, L45
- Panter B., Heavens A. F., Jimenez R., 2004, *MNRAS*, 355, 764
- Piran T., 2004, *RvMP*, 76, 1143
- Porciani C., Madau P., 2001, *ApJ*, 548, 522
- Porciani C., Madau P., 2000, *ApJ*, 532, 679
- Preece R. D., Briggs M. S., Mallozzi R. S., Pendleton G. N., Paciasas W. S., Band D. L., 2000, *ApJS*, 126, 19
- Rowan-Robinson M., 1999, *Ap&SS*, 266, 291
- Sakamoto T., et al., 2008, *ApJS*, 175, 179
- Sakamoto T., et al., 2009, *ApJ*, 693, 922
- Salvaterra R., et al., 2008, *IAUS*, 255, 212
- Salvaterra R., Chincarini G., 2007, *ApJ*, 656, L49
- Salvaterra R., Guidorzi C., Campana S., Chincarini G., Tagliaferri G., 2009, *MNRAS*, 396, 299
- Savaglio S., 2006, *NJPh*, 8, 195
- Schmidt M., 2001, *ApJ*, 552, 36
- Soderberg A. M., et al., 2004, *Natur*, 430, 648
- Starling R. L. C., Wijers R. A. M. J., Hughes M. A., Tanvir N. R., Vreeswijk P. M., Rol E., Salamanca I., 2005, *MNRAS*, 360, 305
- Stern B. E., Tikhomirova Y., Kompaneets D., Svensson R., Poutanen J., 2001, *ApJ*, 563, 80
- Stern B. E., Tikhomirova Y., Svensson R., 2002, *ApJ*, 573, 75
- Tanvir N. R., et al., 2009, *Natur*, 461, 1254
- Totani T., 1997, *ApJ*, 486, L71
- Virgili F. J., Liang E.-W., Zhang B., 2009a, *MNRAS*, 392, 91
- Virgili F. J., Zhang Bing, O'Brien P., Troja E., 2009b, *ApJ*, submitted (arXiv:0909.1850)
- Wanderman D., Piran T., 2009, arXiv, arXiv:0912.0709
- Wang F. Y., Dai Z. G., 2009, *MNRAS*, 400, L10
- Wijers R. A. M. J., Bloom J. S., Bagla J. S., Natarajan P., 1998, *MNRAS*, 294, L13
- Wolf C., Podsiadlowski P., 2007, *MNRAS*, 375, 1049
- Woosley S. E., 1993, *ApJ*, 405, 273
- Woosley S. E., Bloom J. S., 2006, *ARA&A*, 44, 507
- Yüksel H., Kistler M. D., 2007, *PhRvD*, 75, 083004
- Yoon S.-C., Langer N., 2005, *A&A*, 443, 643
- Zhang B., 2007, *ChJAA*, 7, 1
- Zhang B., et al., 2007, *ApJ*, 655, 989
- Zhang B., Mészáros P., 2004, *IJMPA*, 19, 2385

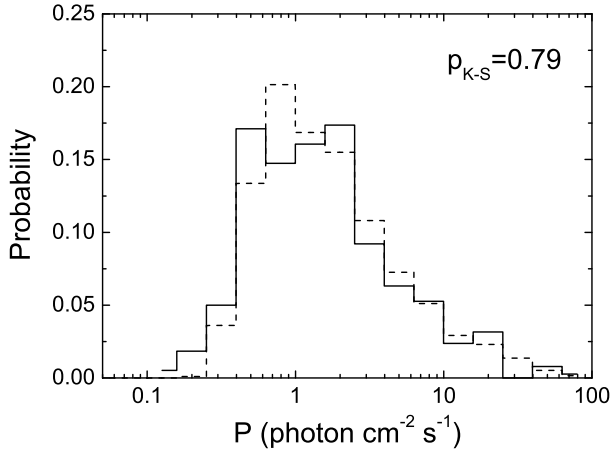


Figure 1. Comparison of the peak flux distribution of LGRBs detected by BATSE (dashed line) to BAT GRB sample (solid line). BATSE data are from Stern et al. (2001) and BAT data are from NASA website. The peak fluxes of the BATSE GRBs are converted to the BAT energy band of [15, 150] keV for comparison, with a typical spectral parameter set of $\Gamma_1 = 0.83$, $\Gamma_2 = 2.35$ and $E_p = 302$ keV.

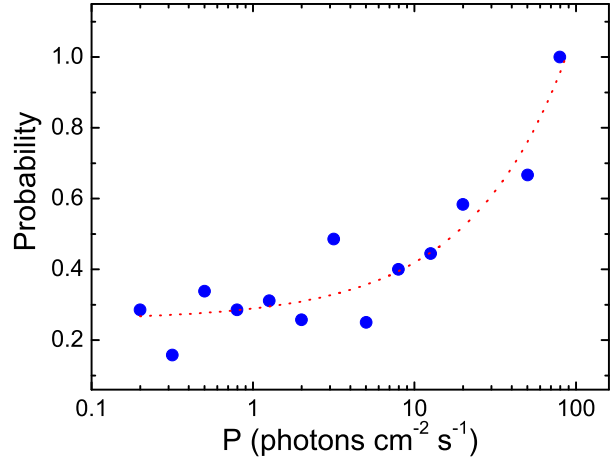


Figure 3. Redshift measured probability as a function of the peak flux with our best fit (dotted curve) for BAT LGRBs. The best fit curve is parameterized in Eq. 10.

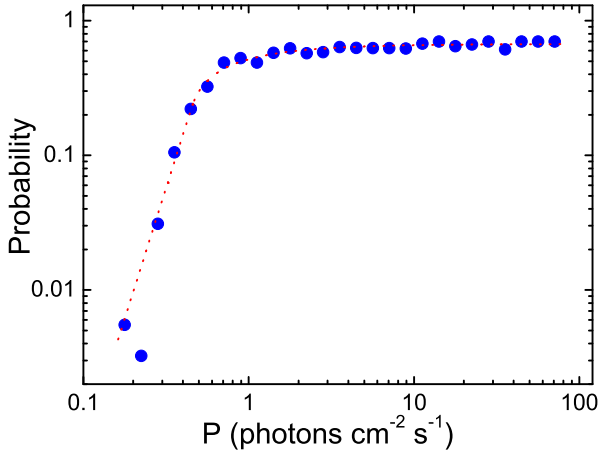


Figure 2. Trigger probability as a function of the peak flux with our best fit (dotted curve) for BATSE LGRBs. The best fit curve is parameterized in Eq. 9.

Table 1. The selected model parameters from our simulations and the corresponding K-S test probability.

Case	Model parameters ^a				K-S test ^b					
	ϵ	δ	$\rho_0^{\text{LL}}/\rho_0^{\text{HL}}$	α_2^{HL}	$p_{\text{K-S}}^P$		$p_{\text{K-S}}^z$		$p_{\text{K-S}}^L$	
A	–	–	50	2.5	0.423	0.585	< 0.001	< 0.001	< 0.001	0.005
B	0.5	–	50	2.2	0.372	0.449	0.033	0.009	0.052	0.292
C	–	0.85	300	2.0	0.258	0.889	0.060	0.242	0.018	0.369
D	0.4	0.4	200	2.0	0.698	0.993	0.294	0.843	0.209	0.966

Note: ^a The parameters of the luminosity function of LL-GRBs are fixed at $\alpha_1^{\text{LL}} = 0$ and $\alpha_2^{\text{LL}} = 3.0$, $L_b^{\text{LL}} = 7.5 \times 10^{46}$ erg s⁻¹. For HL-GRBs, L_b^{HL} also fixed at 2.75×10^{52} erg s⁻¹ and α_1^{HL} fixed at 1.36. ^b From *left to right*: The K-S test probabilities of $\log N - \log P$, $\log(1+z)$, and $\log L$ distributions (triggered GRBs | z -known sample).

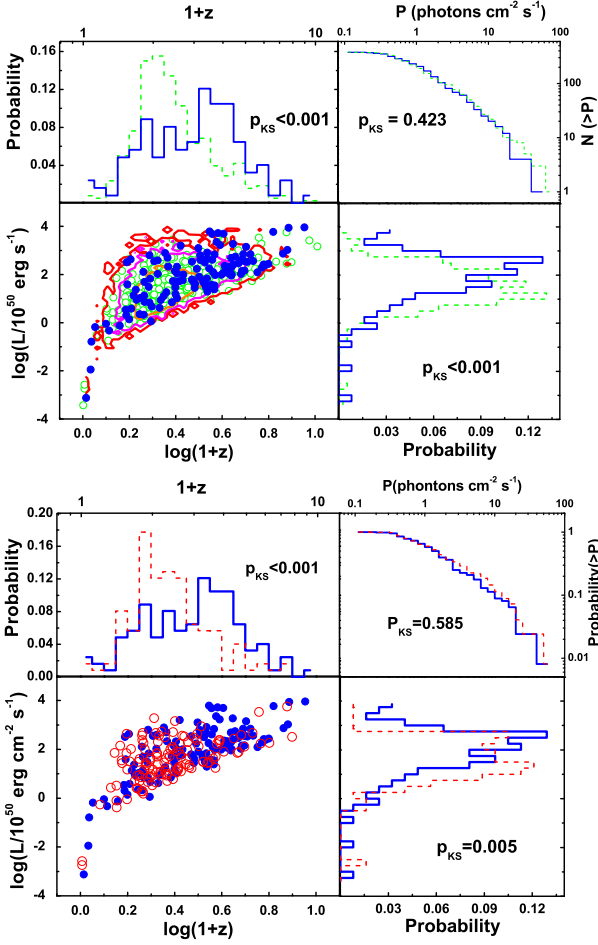


Figure 4. Comparisons of two-dimensional $\log L - \log z$ distributions and one-dimensional $\log L$, $\log z$, and $\log P$ (accumulative $\log N - \log P$) distributions between the observed *Swift*/BAT GRB sample (solid dots and solid lines) and our simulations (open dots and dashed lines) for Case A: $R_{\text{LGRB}}(z) \propto R_{\text{SFR}}(z)$. *left four panels* are for the triggered GRB sample. The contours in the $\log L - \log z$ plane show the relative probability distributions of the simulated GRBs with different color lines: red for 99.7%, magenta for 95.5%, and orange for 68.7%. *Right four panels* are for the sample with redshift measurement. One dimensional K-S test probabilities for the comparisons are marked in each panel.

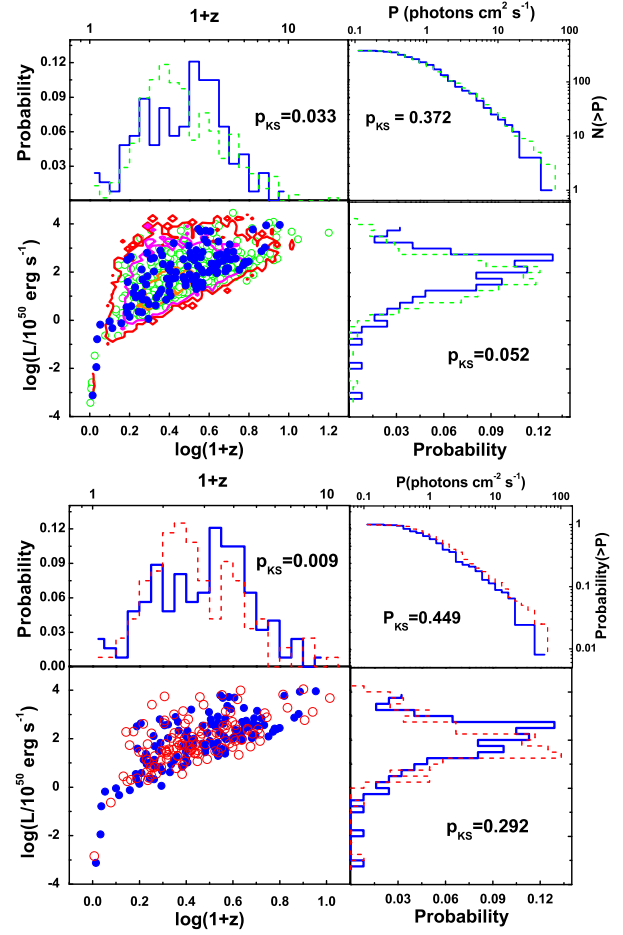


Figure 5. The same as Fig. 4, but for Case B: $R_{\text{LGRB}}(z) \propto R_{\text{SFR}}(z)\Theta(\epsilon, z)$.

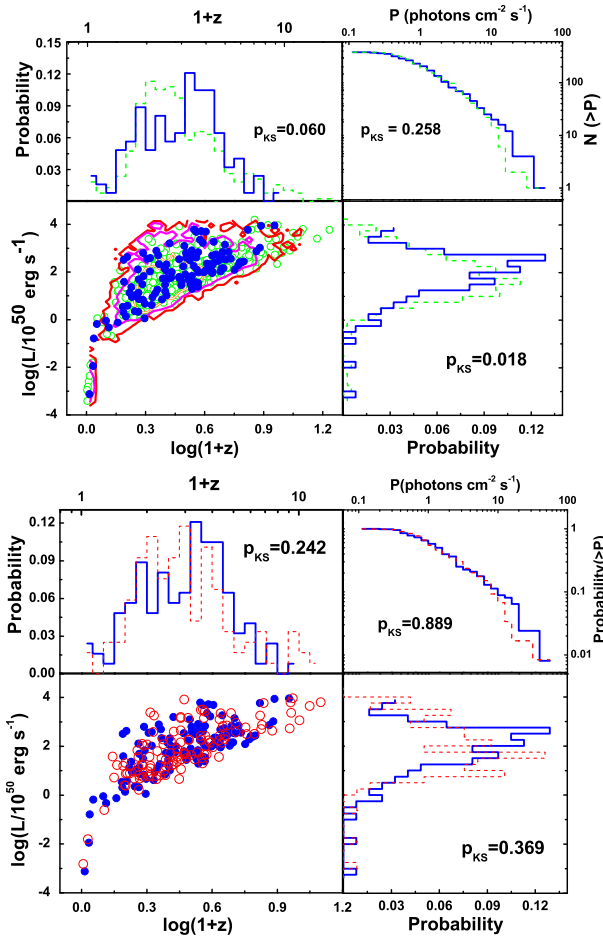


Figure 6. The same as Fig. 4, but for Case C: $R_{\text{LGRB}}(z) \propto R_{\text{SFR}}(z)(1+z)^\delta$.

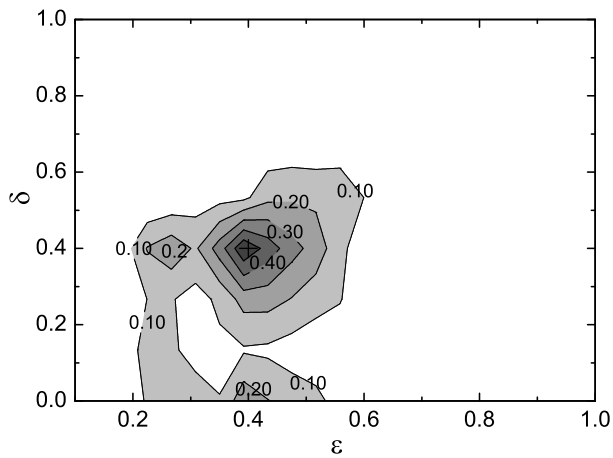


Figure 7. Contours of p_{K-S} in the $\epsilon - \delta$ plane for Case D: $R_{\text{LGRB}}(z) \propto R_{\text{SFR}}(z)(1+z)^\delta \Theta(\epsilon, z)$, where $p_{K-S} = p_{K-S}^P \times p_{K-S}^z \times p_{K-S}^L$. The p_{K-S}^P , p_{K-S}^z , and p_{K-S}^L are the probabilities of the K-S tests for the $\log N - \log P$, z , and L distributions of the simulated GRB sample with redshift measurement, respectively. The cross marks the best consistency between our simulations and observations, i.e., $(\delta, \epsilon) = (0.4, 0.4)$.

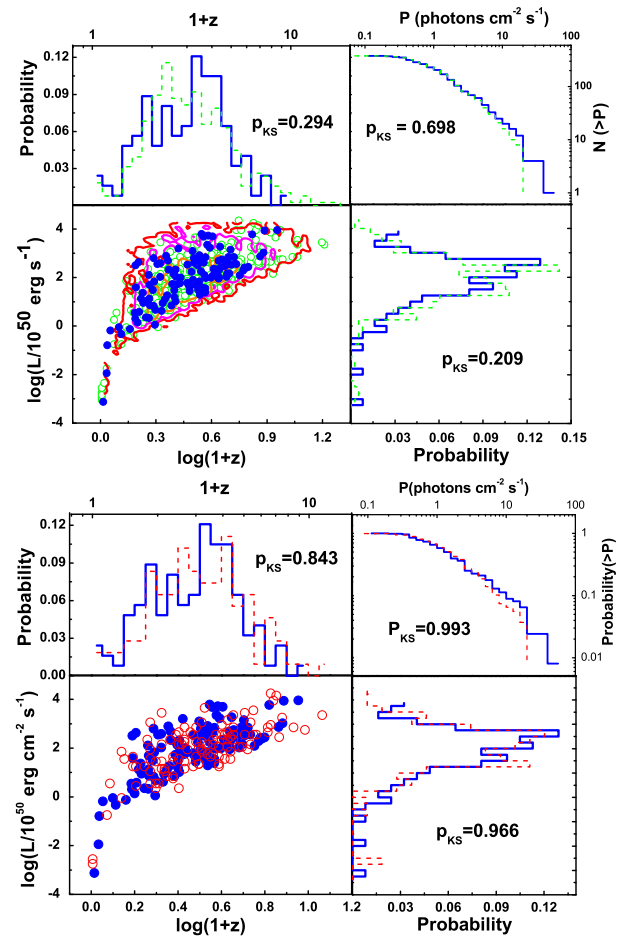


Figure 8. The same as Fig. 4, but for Case D: $R_{\text{LGRB}}(z) \propto R_{\text{SFR}}(z)(1+z)^\delta \Theta(\epsilon, z)$.

with a parameter set $(\delta, \epsilon) = (0.4, 0.4)$.